Applied Energy 188 (2017) 444–455

Contents lists available at ScienceDirect

Applied Energy

journal homepage: www.elsevier.com/locate/apenergy

# Decentralized control of a scalable photovoltaic (PV)-battery hybrid power system

Myungchin Kim [a], Sungwoo Bae [b,*]

[a] Agency for Defense Development, Daejeon 34186, South Korea
[b] Department of Electrical Engineering, Yeungnam University, Gyeongsan-si 38541, South Korea

## HIGHLIGHTS

- This paper introduces the design and control of a PV-battery hybrid power system.
- Reliable and scalable operation of hybrid power systems is achieved.
- System and power control are performed without a centralized controller.
- Reliability and scalability characteristics are studied in a quantitative manner.
- The system control performance is verified using realistic solar irradiation data.

## ARTICLE INFO

*Article history:*
Received 9 September 2016
Received in revised form 5 December 2016
Accepted 8 December 2016

*Keywords:*
Hybrid power system
Power management
Standalone energy system
Solar-battery system

## ABSTRACT

This paper presents the design and control of a sustainable standalone photovoltaic (PV)-battery hybrid power system (HPS). The research aims to develop an approach that contributes to increased level of reliability and scalability for an HPS. To achieve such objectives, a PV-battery HPS with a passively connected battery was studied. A quantitative hardware reliability analysis was performed to assess the effect of energy storage configuration to the overall system reliability. Instead of requiring the feedback control information of load power through a centralized supervisory controller, the power flow in the proposed HPS is managed by a decentralized control approach that takes advantage of the system architecture. Reliable system operation of an HPS is achieved through the proposed control approach by not requiring a separate supervisory controller. Furthermore, performance degradation of energy storage can be prevented by selecting the controller gains such that the charge rate does not exceed operational requirements. The performance of the proposed system architecture with the control strategy was verified by simulation results using realistic irradiance data and a battery model in which its temperature effect was considered. With an objective to support scalable operation, details on how the proposed design could be applied were also studied so that the HPS could satisfy potential system growth requirements. Such scalability was verified by simulating various cases that involve connection and disconnection of sources and loads. The quantitative reliability analysis and verification results show that the proposed architecture with power control strategy provides a straightforward approach for designing a reliable and scalable PV-Battery HPS. Although PVs and batteries have been used in this paper, the design and control approach can be applied to other hybrid power systems (HPSs) that involve the connection of various power sources.



## 1. Introduction

There is a dire demand to ensure reliable power supply for sustainable growth. In order to address this demand, hybrid power systems (HPSs) have been adopted for various applications. Representative examples of power sources in an HPS include photovoltaic (PV) modules [1–3], wind turbines [4–6], fuel cells [7,8], batteries [9,10], and supercapacitors [11,12]. The installation of different types of power sources can decrease the probability that a power system could be affected by unmanageable operational constraints (e.g., environmental conditions, fuel supply options). However, the sizing of power sources and design of power control algorithms should still be conducted in a comprehensive manner to ensure stable operation for various operating scenarios. Examples of objectives to be accomplished by system

* Corresponding author.
*E-mail address:* sbae@yu.ac.kr (S. Bae).

http://dx.doi.org/10.1016/j.apenergy.2016.12.037
0306-2619/

control approaches include maintaining the power balance and ensuring that energy storage devices are not exposed to operation conditions that lead to performance degradation. Since an HPS is operated with various power sources connected to the system, the design of system architecture with control for a HPS is not a trivial task. For example, intermittent characteristics of renewable sources and slow response speed of fuel cells [10] can cause either short-term or long-term power imbalance. Although the installation of energy storage can be the most intuitive approach to solve power imbalance issues, additional challenges caused by operational or safety requirements of different energy storage technologies can increase the level of complexity in the energy management [12,13]. Compliance with such requirements (e.g., charge rate, depth-of-discharge) has a nontrivial effect on the performance and life periods of the energy storage [13].

Architectures and control approaches for a standalone HPS have been researched on both stationary [1,4,5] and onboard power systems [8,9]. Centralized control approaches have been studied for a power system that consists of renewable sources and an energy storage device [4,14]. In such approaches, the system transits its operation mode depending on the relationship between the available power and the load power. The renewable sources (i.e., PV modules and wind turbines) change the operation mode depending on the power balance of the power system, while the energy storage is used to ensure power balance. A system control approach for an HPS with PV plants, batteries, and supercapacitors has been explored for grid-connected applications [15]. The proposed rule-based controller performs power sharing by changing the command value for each power source depending on the operation mode. Predictive control approaches have also been applied for power management in PV-Battery HPS [16] and PV-wind-diesel-battery HPS applications [17]. By utilizing the predicted information of the power system (e.g. load demand and output power), the HPS power flow is controlled to achieve satisfactory operation. The combination of a battery and a fuel cell has also been adopted to power an electric drive system [8,10]. This hybrid system is controlled such that the battery handles the power imbalance during the transient period to mitigate the slow response of the fuel cell. An approach that controls the operating pressure of the fuel cell in a fuel cell-battery power system was also proposed [7]. The control strategy enables active power sharing between the fuel cell and the battery. The study of [9] proposed using the state-of-charge (SOC) level to generate reference commands for fuel cells in a fuel cell-battery HPS. Results of proportional-integral (PI) and fuzzy logic control that use the feedback of the battery SOC information demonstrated the applicability of such a power system in hybrid vehicles. Studies on an HPS for public buses [11,18,19] and unmanned aerial vehicles [20,21] also showed that an HPS can demonstrate satisfactory performance for most practical mission profiles. Furthermore, benefits such as cost effective operation and optimal use of energy storage can be achieved through the optimized design of system architecture with control for a PV-integrated HPS [1,2,22].

This paper introduces the design and control of a PV-battery HPS that effectively addresses the challenges caused by the intermittent output of PV sources. Especially, emphasis has been placed on achieving a high level of reliability and scalability. As HPSs require connection of various power sources, the operation characteristics of the overall power system would be affected by how the system hardware is configured and how the different power sources are controlled. Accordingly, this paper proposes an approach for a system architecture with control for a PV-battery HPS operating in a standalone configuration. The battery is directly connected to the system main bus (i.e., passive configuration) in order to realize a reliable and cost effective design [7]. The possible advantages of such a design approach from a hardware reliability perspective are studied by performing a quantitative reliability analysis using failure rates of previous studies. Compared with studies on controller design [4,14], system architecture [23] and efficiency analysis [24], research on the quantitative reliability performance for an HPS with a passively connected battery seems to be rather limited. This paper proposes a system control approach for an HPS with a passive configuration that does not require a centralized supervisory control unit or algorithm. That is, the proposed system can be controlled without explicit feedback of loads and does not require a separate supervisory controller. Because the exchange of information or commands among sources, loads, and the controller is not required, the burden for implementing stable communication paths can be relieved. In addition, with an objective to achieve the maximum life cycle, the proposed control approach considers the operational requirements of the energy storage. In particular, this study focuses on the requirement that the charge rate of the battery should be limited, which is a requirement that was not thoroughly explored in the past research works on the control of an HPS with a passive configuration [21]. Such design features allow the proposed approach to be a more reliable and robust design alternative for an HPS with passive configurations. Furthermore, the proposed approach for system architecture with control enables scalable design of an HPS. The system size can be easily increased or decreased in a straightforward manner such that it does not require significant efforts for hardware and software modifications. Such scalable operation behavior is possible, as the system does not rely on a centralized supervisory controller and extensive communication between various units (i.e., sources and loads) of the HPS. As the system is easily scalable, changes in the system size can be performed with minimal effort. Necessary activities to be performed as a result of the system size changes are limited to local activities such as connection/disconnection of the hardware unit and control logic updates for the corresponding unit without modifications to the rest of the HPS. Not only the system is scalable, but also the proposed power management approach ensures that the PV modules share the load demand with respect to power ratings. While research works on the considered power architecture (i.e., HPS with a passive connection of energy storage) have been reported in various studies, most research works have only focused on how to control the power flow during different operation conditions [4,14] or have not provided sufficient discussions on the effect of future source connection to system performance [9,20,21,25].

The rest of this paper is organized as follows. Section 2 illustrates the system architecture. The characteristics of the power system architecture are also discussed. Section 3 initiates the operation of the HPS with the proposed control approach. The system design and performance of the HPS with multiple PV sources are discussed in Section 4. The simulation results of the power system and control strategy are shown in Section 5, while Section 6 provides a concluding remark on the study.

## 2. HPS architecture

This study investigates the improvement of the existing works on the architecture of HPSs. As shown in Fig. 1, the HPS of this paper consists of PV sources, energy storage, and loads. Although the proposed HPS control scheme can also be applied to a grid-connected configuration, the scope of this paper is limited to a standalone configuration such as a remote telecommunication power system for the simplicity of the analysis. The proposed system can also be used as a back-up power system for critical facilities such as data centers and hospitals when a power outage occurs in the utility grid. While such secure facilities could operate with the power supplied from the utility grid during normal situations,

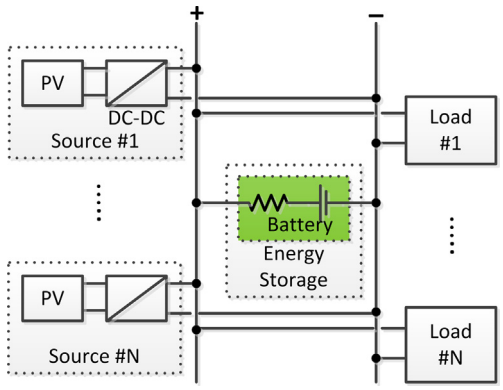


**Fig. 1.** Considered architecture of the PV-battery HPS.

the power source could be changed from the utility grid to the HPS in case of grid outages. In such a situation, both the PV sources and the energy storage would work as a secondary source to prevent power loss for critical infrastructures. Even in case the PV sources are not available, the energy storage could work as a power source for such a case. Because the proposed power system is not connected to a stiff source (e.g., electric power grid), maintaining a balanced power flow between the entities (i.e., sources, energy storage, and load) of the HPS is critical for ensuring system stability [26].

### 2.1. PV sources

The mathematical modeling of PV sources in which the PV panel with its power electronic interface (PEI) is connected as shown in Fig. 1 can be explained as follows. As shown in Fig. 1, a PV source in this paper is defined as a PV panel with a power electronic interface (PEI), which is normally a DC-DC converter. In order to ensure that the PV sources provide the maximum possible power, it is common to apply algorithms that force the PV source to operate at the maximum power point (MPP). While the MPP tracking algorithm can strongly affect the dynamic response performance of PV panels, the power output of the PV sources is likely to be affected by external factors such as solar irradiance and temperature. Based on the assumption that PV sources operate at the MPP with a PEI, the output voltage and current of the solar modules are modeled by a simplified mathematical model that captures the effect of changes in the solar irradiance and temperature as [27–29] given by

$$V_{mpp}(G,T) \approx V_{mpp,n} + K_v \cdot (T - T_n), \tag{1}$$

$$I_{mpp}(G,T) \approx \frac{G}{G_n} I_{mpp,n} + K_i \cdot (T - T_n) \tag{2}$$

where $V_{mpp}(G,T)$ and $I_{mpp}(G,T)$ are respectively the maximum output voltage and current of the PV sources with functions of solar irradiance ($G$) and temperature ($T$), $V_{mpp,n}$ and $I_{mpp,n}$ are respectively the PV maximum output voltage and current at the nominal test condition (i.e., 1000 W m$^{-2}$, 25 °C) from a PV datasheet, $K_v$ and $K_i$ are respectively the temperature coefficients of a PV open circuit voltage ($V_{oc}$) and a PV short circuit current ($I_{sc}$) which can be found in the PV datasheet, $T_n$ is the nominal test temperature (i.e., 25 °C), and $G_n$ is the solar irradiance of the nominal condition (i.e., 1000 W m$^{-2}$). Eqs. (1) and (2) can be derived by the assumption that the series resistance and the parallel resistance of the PV sources are respectively zero and infinite. This assumption is true because the series and parallel resistance of a commercial PV module are usually low and high enough respectively [25].

From Eqs. (1) and (2), the power output of PV sources operating at the MPP can be calculated as

$$P_{mpp}(G,T) = \eta \cdot V_{mpp}(G,T) \cdot I_{mpp}(G,T) \tag{3}$$

where $P_{mpp}(G,T)$ is the maximum output power of the PV sources at a certain solar irradiance ($G$) and temperature ($T$), and $\eta$ is the power conversion efficiency of an overall PV source system including a PV panel and a PEI attached to a PV panel. Modeling PV sources based on Eqs. (1)–(3) may not be able to capture the transient response of the PV sources to changes in external factors. However, such an approach is still sufficient to be used during the system sizing process because it provides the maximum power value of PV sources, which are intermittent power sources. Alternative modeling approaches of PV sources can be found in [27,30].

### 2.2. Energy storage

The power insecurity associated with the PV sources could be eliminated by the HPS mechanism that effectively addresses the power imbalance between sources and loads. Examples of the characteristics that could cause a power imbalance include the intermittent output of PV sources and pulsed load profiles. Because an HPS usually involves the installation of various sources with different response characteristics, this study considers energy storage installation as a solution to address potential power imbalance issues.

In the power architecture of this study, the power mismatch is addressed by directly connecting the battery to the main system bus as shown in Fig. 1, similar to power systems for telecommunication sites [31]. Such a configuration, which is also known as a passive configuration [7], was selected based on the effect that the installation of PEIs would have on system size, cost, efficiency and reliability. It is worth noting that such factors could be critical to the integration process of not only stationary applications (e.g., data centers) but also mobile platforms such as electric vehicles [10]. It is rather evident that the installation of additional PEIs might result in increased system cost and larger physical dimensions (e.g., size and weight). The PEI would also introduce additional power losses, such as the conduction losses and switching losses of power electronic devices. While the effect of PEIs to system efficiency can be minimized by applying advanced switching technologies [32] and novel power switching devices [33], such losses are still expected to exist.

Regarding the effect of PEIs to system reliability, PEIs can be viewed as a collection of passive and active electronic components that wear out or can even fail [34]. In case the energy storage is connected to the system through a dedicated PEI, the power flow between the storage device and the rest of the system could be possible only through the PEI. With such a configuration feature, it is possible that the energy storage could not solve the power imbalance issues because of a fault in the PEI regardless of the operation status of the energy storage. As sustained operation of an HPS with a power imbalance would lead to system failure, the reliability of the overall HPS is expected to be dependent upon failure rates of not only the energy storage but also the PEI.

Fig. 2 shows how the HPS reliability value is affected by the PEI failure rate. In Fig. 2, case 1 corresponds to an HPS configuration without a PEI for energy storage (i.e., directly-connected storage) whereas cases 2 and 3 represent HPS configurations that use a PEI for connecting the energy storage to the system main bus. To plot Fig. 2, a constant failure rate reliability model was assumed as [29]

$$R(t) = \exp(-\lambda t) \tag{4}$$

where $\lambda$ is the failure rate. The reliability function of the HPS without the PEI can be written as

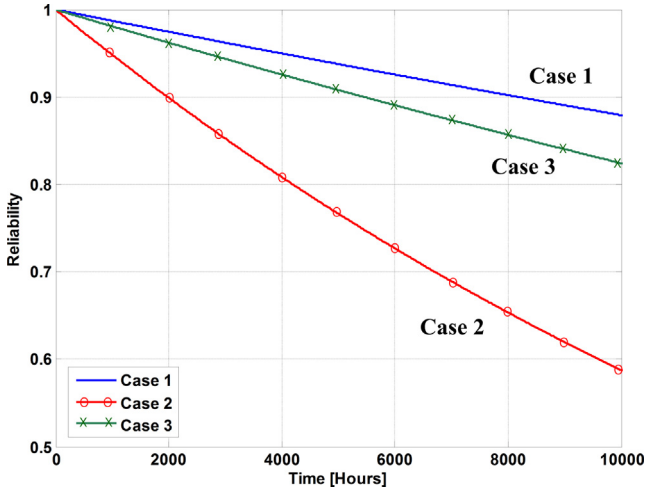


**Fig. 2.** Results of a hardware reliability analysis.

$$R_1(t) = \exp(-\lambda_b t) \tag{5}$$

where $\lambda_b$ is the failure rate of the battery. In case the PEI is used for connecting the energy storage, the reliability block diagram of the system has a series structure [35] that could be modeled as a cascaded connection of the energy storage and the PEI. That is, both the energy storage itself and the additional PEI are required to be operational for the energy storage to perform power balancing between the PV sources and the load. Then, the reliability function of the HPS with the additional PEI can be written as

$$R_2(t) = [\exp(-\lambda_b t)] \cdot [\exp(-\lambda_{pei} t)] = \exp[-(\lambda_b + \lambda_{pei})t] \tag{6}$$

where $\lambda_{pei}$ is the failure rate of the PEI. As an illustrative example, the failure rate data of [34] were used as $\lambda_b = 12.89 \times 10^{-6}$ failures per hour and $\lambda_{pei} = 40.29 \times 10^{-6}$ failures per hour. Since most PEIs share similar hardware components (e.g., solid-state switches, capacitors, and inductors), whether the PEI performs DC-DC or DC-AC power conversion would not be a critical factor affecting the reliability analysis as long as the number of power conversion stages and the component ratings are similar.

As shown in Fig. 2, the hardware reliability value of the HPS is affected by the additional installation of PEIs. Such an effect can be observed by comparing case 1 and case 2. The decrease in the reliability value can be explained by the higher hardware part count of case 2 compared with that of case 1. Although the failure rate of the PEI can be decreased by using high quality devices with sufficiently large operation ratings, it is evident from Eqs. (5) and (6) that the HPS reliability would still be affected by the PEI failure rate. In fact, case 3 of Fig. 2 shows the HPS reliability when a hypothetical PEI failure rate that is smaller than the battery failure rate is assumed ($\lambda_{pei} = 0.5\lambda_b$). Such a hypothetical case has been considered to study how the system reliability would change when the failure rate of the PEI is lower than that of the battery. Although case 3 has a higher reliability value compared with case 2, case 1 (HPS without an additional PEI) still has the highest value among the three cases. Such an analysis result shows that the additional PEI used for an energy storage connection could be a critical factor that affects reliability performance of the overall HPS. The system reliability value of the HPS after operating 10,000 h was calculated as in Fig. 3 using various failure rate values of the PEI and the battery. While the failure rate data of [34] were used for earning the result of Fig. 2, a broader range of failure rates were considered in Fig. 3. In case the battery is connected to the HPS through a PEI, the reliability of the overall system is affected by not only the failure rate of the battery but also that of the PEI. Even for a

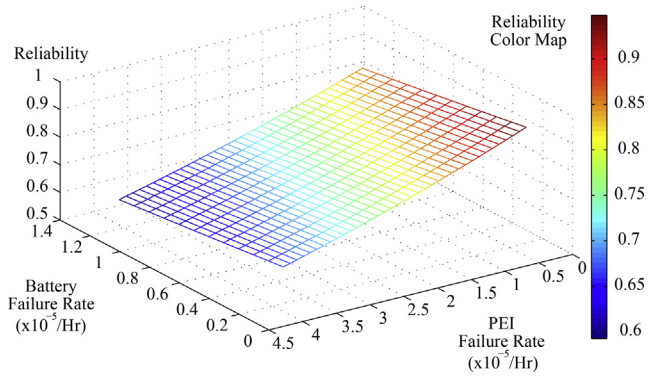


**Fig. 3.** System reliability with different failure rate values.

fixed battery failure rate, the results of Fig. 3 show that the system reliability decreases as the PEI failure rate increases. From Figs. 2 and 3, it could be concluded that the passive configuration used in this study (i.e., configuration without using a dedicated battery power converter) could prevent the HPS operation from being affected by the failure rate characteristics of the PEI. Further details on the characteristics of the adopted energy storage configuration can be found in [31].

## 3. System operation and control design

### 3.1. PV source control

In this study, the PV source operates in either the MPP mode or the Power Regulation (PR) mode. Depending on the power balance and SOC level of the battery, the PV module is controlled to change its operation mode. In the MPP mode, the PV module is forced to generate the maximum possible power. In other words, the output power of the PV module operating in the MPP mode is expected to follow Eq. (3). In order to achieve power balance for cases where the load power is smaller than the output of PV sources, this study also defined the PR mode, in which the output of the PV power is regulated to a value that is lower than the maximum available power. Fig. 4 shows the block diagram of the PV control module. Instead of using the load power information as an indicator for mode transition, the battery current information is compared with a pre-defined threshold value for determining the necessity of mode transition. Such an approach contributes to increasing system reliability by reducing the communication and computation burden for acquiring the consumed load power information.

### 3.2. System operation

The operation of the system can be explained by considering the power balance between the PV modules and loads.

In case the PV power level is sufficient to power the load, the PV source operates in the MPP mode so that the discharge of energy storage is minimized. While the surplus power (i.e., difference between the generated power of the PV source and the consumed power of the load) is used to charge the energy storage, the PV source transits to the PR mode when the charge rate of the energy storage exceeds the pre-defined threshold value. In the case of the storage configuration of Fig. 1, the operation mode of the PV source is determined by the battery charge current. In this study, the power command ($P^*$) for the PV source operating in the PR mode is generated as

$$P^* = P_{mpp} - n(i_B - I_{BS}) \tag{7}$$

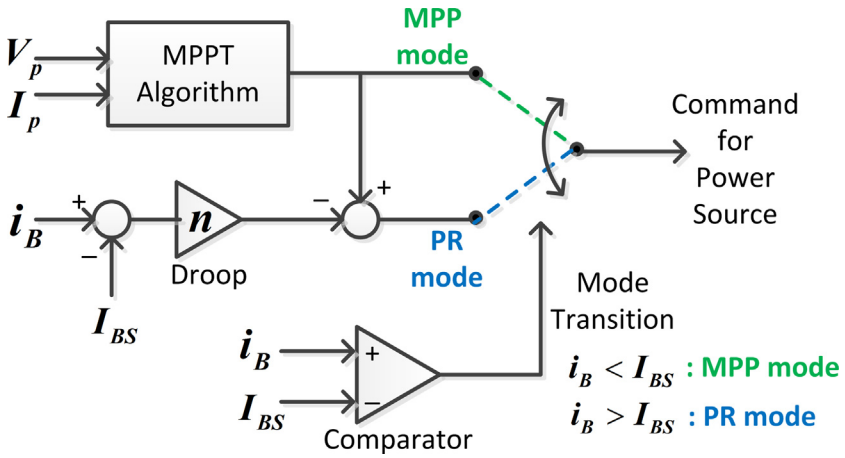


**Fig. 4.** Block diagram of the PV control module.

where $P_{mpp}$ is the maximum power, $n$ is the droop gain, $i_B$ is the battery charging current, and $I_{BS}$ is a control variable that is selected by a system designer. The concept of drooping power commands has been reported as a decentralized approach in past studies for enabling load sharing between different power sources in microgrids [36] and preventing occurrence of overvoltage by grid connected distributed generation sources [37]. In this study, such an approach was used with an objective to perform power management of a standalone HPS and prevent the DC bus battery from experiencing an uncontrollable rise of charging rate caused by the intermittent nature of the PV sources and dynamic load profiles.

The detailed operation principle of Eq. (7) can be explained from Fig. 5. It can be seen that the power command of the PV source starts to decrease from the maximum available power value, $P_{mpp}$, once the battery current is larger than the control variable $I_{BS}$. Initially, the PV source operates at point A in which the PV power is the maximum power value, $P_{mpp}$, for the battery current $I_{B1}$. At point A, the power generated by the PV source is equal to the sum of the load power and the battery charging power. In case the power system experiences a decrease in the load power, the power system experiences an operation point transition from point A to point B. While the output power of the source is identical at point A and point B, the battery current increases from $I_{B1}$ to $I_{B2}$, caused by the sudden load power decrease. The increase in the battery current can be explained from the power relationship between the source, the energy storage, and the load as

$$P_B = V_B \cdot i_B = P_S - P_L \tag{8}$$

where $P_B$ is the battery power, $V_B$ is the battery terminal voltage, $i_B$ is the battery charging current, $P_S$ is the supplied power, and $P_L$ is the load power.

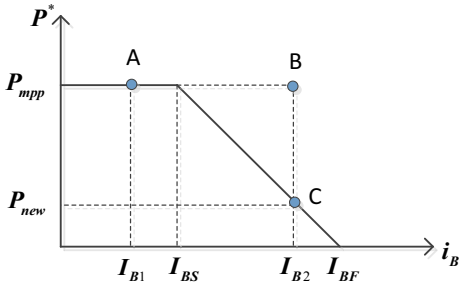


**Fig. 5.** Illustration of the droop law (Eq. (7)).

Once the battery current is higher than the threshold battery value, $I_{BS}$ of Eq. (7) and Fig. 5, the PV source switches to the PR mode and the power command is reduced to $P_{new}$. Such a change can be represented as a transition from point B to point C in Fig. 5. As the power relationship between sources, loads, and energy storage holds as Eq. (8), further increase in the battery current is prevented by the decrease in the PV output power.

As shown in Eq. (7), the system performance is decided by the values of the control parameters, $n$ and $I_{BS}$. While $n$ determines how fast the power command value decreases as the battery current increases, $I_{BS}$ is the battery current threshold value that causes the power command to decrease. In this paper, the droop gain ($n$) is determined by the maximum output of the PV source ($P_{mpp}$) and the maximum allowable battery current (i.e., $I_{BF}$ of Fig. 5). That is,

$$n = \frac{P_{mpp}}{I_{BF} - I_{BS}}. \tag{9}$$

The battery current cannot exceed the $I_{BF}$ value because the power command value of the PV source linearly decreases to zero as the battery current increases to $I_{BF}$. Since no external power will be available when the battery current is $I_{BF}$, the battery current cannot exceed the battery current limit value as long as a load is connected.

It is worth noting that the safety, life cycle, and performance of a battery depend on how well the battery is managed [13]. In particular, it is important that occurrences of excessively high battery current values should be avoided to prevent side effects caused by internal impedance and heat of the battery [38]. As a result of such battery heat, a rise in the battery temperature is expected to occur according to the dynamic model of the battery temperature as [39]

$$C_b \frac{dT_b}{dt} = Q_b - k \cdot (T_b - T_S) \tag{10}$$

where $C_b$ is the battery thermal capacity, $T_b$ is the battery temperature, $Q_b$ is the battery heat generation, $k$ is the heat conduction coefficient, and $T_S$ is the battery shell temperature. Since the battery temperature is a major factor that affects the overall battery performance (e.g., reliability and capacity), it is generally recommended to prevent batteries from experiencing high operation temperatures and abrupt temperature rises [13,40]. While specific requirements may differ depending on the battery technology type [40], such management functions are commonly implemented in battery charging circuits [38] and battery management systems (BMS) [41].

In case the load demand is higher than the generated power of PV modules, both the PV modules and the battery supplies the power to meet the load demand. Such a situation can happen because of a decrease in PV output power caused by irradiance variation [42] and partial shading [43]. In this case, the PV modules operate in the MPP mode to minimize discharge of the battery. In case the SOC level reaches the minimum SOC limit value of the battery, then part of the loads are shed. This is to prevent the battery from experiencing deep discharge cycles, which is one of the well-known causes of shortening the remaining life period of batteries [13].

### 3.3. Equivalent circuit

The equivalent circuit of the HPS can be modeled as shown in Fig. 6. Because a PV source is not dispatchable due to its intermittent nature, the PV source is controlled to work as a variable current source [44] that feeds power to the main system bus. The magnitude of the current source is determined by the operation mode of the PV modules (i.e., MPP mode or PR mode). Whereas the PV modules supply the maximum available power in the MPP mode, the PV module injects a current value that corresponds to the drooped power command of Eq. (7) in the PR mode. The system bus consists of the energy storage, which balances the power imbalance by either charging or discharging energy according to the instantaneous power difference between sources and loads.

DC power systems or HPSs with high use of renewable energy sources might experience stability problems caused by power imbalance [45] and interaction among various sources and loads that are connected by actively controlled power converters [46,47]. The direct battery connection configuration (i.e., directly connected to the system bus without using a power converter) that is used in this paper contributes to system stability improvement by instantaneously responding (i.e., charging or discharging) to possible power mismatches caused by transitions of operation states or load changes. In fact, the direct battery connection configuration of this study achieves an effect that is equivalent to installing a capacitor with a relatively large capacitance value [48]. As reported in [47,48], increasing the system bus capacitance value is an approach that can handle stability concerns in dc systems with extensive interconnections of power converters. Readers can refer to further detailed studies that have reported the effect of controller parameters [47], load characteristics [48], and operation state transitions [46] on stability management in dc power networks.

## 4. System operation with multiple sources

In case an additional PV module is required to be connected to the HPS, the new source can be easily integrated into the existing system without significant changes to the system. Because a separate centralized supervisory controller that relies on the feedback from other power source information and load power values is not required in this HPS, an expansion of the system to handle possible increase of load power can be performed in a straightforward manner. This section discusses the performance and design approach of the proposed system when additional PV modules are installed. In particular, this paper focuses on the power sharing ratio between different power sources and the battery charge current value.

### 4.1. PV modules with the same power ratings

As the maximum power output ($P_{mpp}$) and the droop gain ($n$) of all modules are identical in the same power rating PV modules case, the same command value will be generated for all PV modules. Hence, it is expected that the PV modules will supply the same amount of power to the load regardless of the battery current value. That is, the PV modules will equally share the power required for the load and the battery.

Under the assumption that the change in the battery terminal voltage caused by the charge/discharge process is negligible, the relationship between the PV generated power, load power, and the battery current can be written as

$$P_{St} = V_B i_B + P_{Lt} \tag{11}$$

where $P_{St}$ is the sum of the PV generated power, and $P_{Lt}$ is the sum of the load power.

As the power output of each PV source is regulated according to the power reference, the sum of the PV generated power is

$$P_{St} = \sum_{i=1}^{N} P_{S,i} = N(P_{mpp} - n(i_B - I_{BS})) \tag{12}$$

where $P_{S,i}$ is the output power of the PV module $i$ and $N$ is the number of PV modules connected to the system.

The effect of an additional source is illustrated in Fig. 7. While the system with a single PV source unit operates at point A with the battery current being $I_{B1}$, the operation point of the system with multiple PV source units shifts to point B with the battery current being increased to $I_{B2}$. In other words, the operation point of the HPS is the intersection point of Eqs. (11) and (12). Hence, the

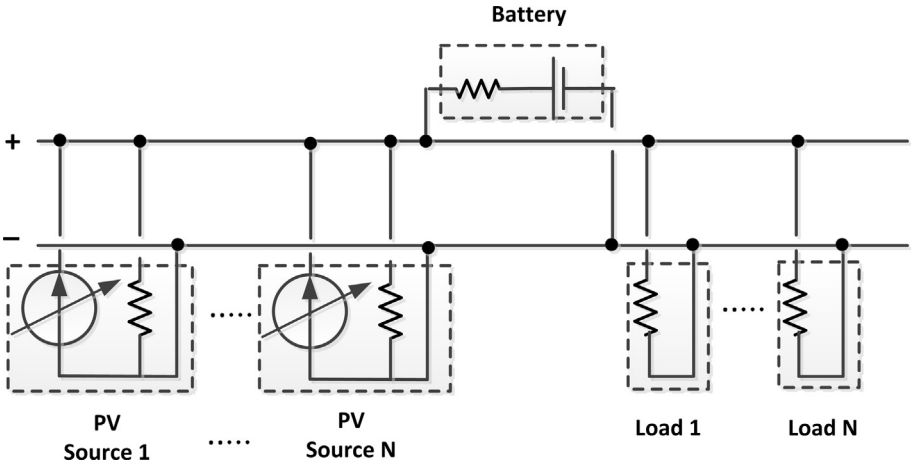


**Fig. 6.** Equivalent circuit of the PV/battery HPS.

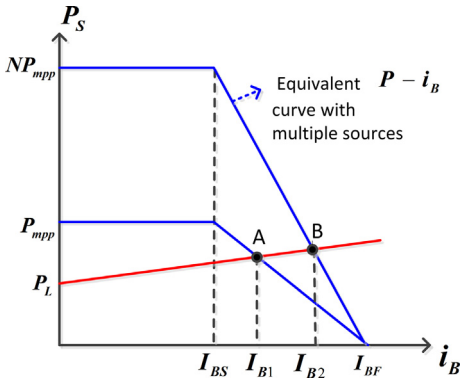


**Fig. 7.** Power-battery current relationship curves.

operation point of the HPS with multiple PV modules can be found by solving

$$P_{St} = NP_{mpp} - nNi_B + nNI_{BS} = V_B i_B + P_{Lt}, \tag{13}$$

and the battery current can be written as

$$i_B = \frac{NP_{mpp} + nNI_{BS} - P_{Lt}}{V_B + nN}. \tag{14}$$

As shown in Eq. (14), it is worth noting that the battery charge current of a HPS with multiple of identical PV modules is determined by the control parameters of the PV module (i.e., $I_{BS}$ and $n$) and the number of PV modules ($N$) that are connected. As the increased battery current should still be lower than the initial design limit value, $I_{BF}$, a constraint on the control parameters, the number of additional power sources, and the load power can be derived as

$$\frac{NP_{mpp} + nNI_{BS} - P_{Lt}}{V_B + nN} < I_{BF}. \tag{15}$$

### 4.2. Power modules with different ratings

In case the PV modules have different ratings, it is desirable that the sources share the load power according to the ratio of power ratings. When the battery current is below $I_{BS}$ (i.e., region I of Fig. 8), the desired load sharing ratio can be achieved as the PV source output is equal to the maximum power output of each module. In addition, the load sharing ratio in region II (i.e., the battery current is larger than $I_{BS}$) can also be preserved as in region I by selecting the droop gain according to Eq. (9). For example, Fig. 8 shows the power command curve for two units, in which the rating

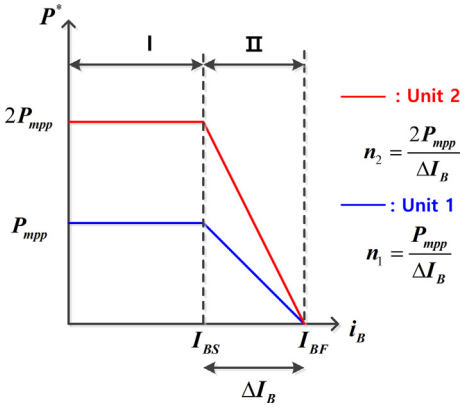


**Fig. 8.** Operation explanation of the power system after a source addition.

of unit #2 is twice larger than that of unit #1. Because the maximum power output of unit #2 doubles that of unit #1, according to Eq. (9), the relationship of the droop gains between the two units can be written as

$$n_2 = \frac{2P_{mpp}}{I_{BF} - I_{BS}} = 2 \cdot \frac{P_{mpp}}{I_{BF} - I_{BS}} = 2n_1 \tag{16}$$

where $n_2$ is the droop gain of unit #2, and $n_1$ is the droop gain of unit #1. It is worth noting that the same $I_{BS}$ value is used for both units. From Eq. (16), the power sharing ratio between the two sources are as

$$\frac{P_2}{P_1} = \frac{2P_{mpp} - n_2(i_B - I_{BS})}{P_{mpp} - n_1(i_B - I_{BS})} = \frac{2P_{mpp} - 2n_1(i_B - I_{BS})}{P_{mpp} - n_1(i_B - I_{BS})} = 2 \tag{17}$$

where $P_1$ is the output power of unit #1 and $P_2$ is the output power of unit #2. As shown in Eq. (17), the power sharing ratio between the two sources is identical to the ratio of power ratings.

## 5. Results and discussions

In order to verify the performance of the proposed HPS architecture and control approach, this study conducted a simulation using MATLAB/Simulink. Fig. 9 shows the power architecture of the HPS considered in the simulation. The voltage level of the system main bus is 60 V, which is established by the battery. As depicted in Fig. 9, the system was assumed to have three PV clusters. While PV clusters 1 and 3 consist of 5 PV modules connected in parallel, PV cluster 2 consists of 10 PV modules. Hence, the power output of PV cluster 2 is twice larger than that of the other two PV clusters. The output of the PV modules was simulated using Eqs. (1) and (2) based on the parameter values of the Kyocera KC 200GT PV module [49]. The specific parameter values of the PV module are shown in Table 1. While the parameter values of Table 1 would vary depending on the characteristics of each PV module product, the performance (e.g., maximum power output) of the PV module is affected by such values. The PV clusters are connected to the system main bus through a switch (i.e., SW 1, SW 2, and SW 3), and

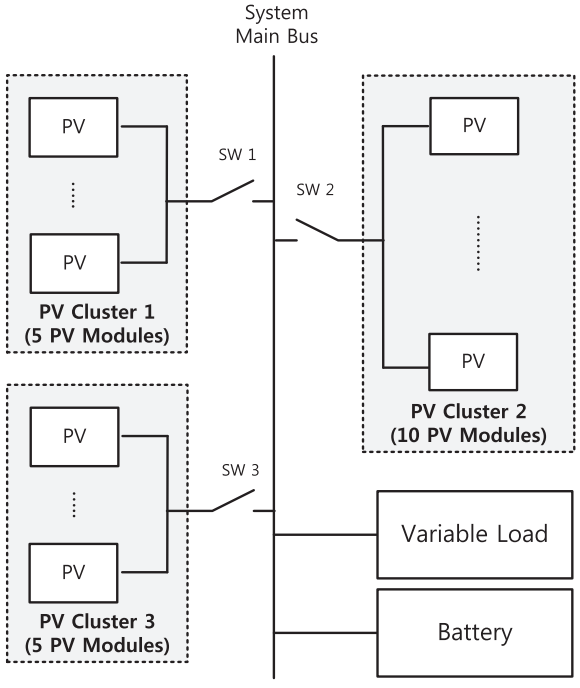


**Fig. 9.** Power architecture of the HPS considered for a simulation study.

**Table 1**
Simulation parameters of a PV module [49].

| Parameter | Value |
|---|---|
| Maximum power voltage ($V_{mpp,n}$) | 26.3 V |
| Maximum power current ($I_{mpp,n}$) | 7.61 A |
| Irradiance at nominal test condition ($G_n$) | 1000 W m$^{-2}$ |
| Temperature at nominal test condition ($T_n$) | 25 °C |
| Temperature coefficient of $V_{oc}$ ($K_v$) | $-1.23{\cdot}10^{-1}$ V °C$^{-1}$ |
| Temperature coefficient of $I_{sc}$ ($K_i$) | $3.18{\cdot}10^{-3}$ A°C$^{-1}$ |

the power conversion efficiency of the overall PV systems was assumed to be 95%. According to Eqs. (9) and (16), the droop gain for each PV cluster 1, 2, and 3 was selected using the maximum power output of each PV cluster and the assumed design parameters (i.e., $I_{BS}$ = 5 A and $I_{BF}$ = 10 A). The maximum output power of PV clusters 1 and 3 is 1000 W, whereas the maximum output of PV cluster 2 is 2000 W. Hence, the droop gain is determined as $n_1 = n_3 = (1000)/(10–5)$=200 W A$^{-1}$ and $n_2 = (2000)/(10–5) =$ 400 W A$^{-1}$.

The simulation results of Fig. 10 show how the system operation can be different depending on the power management strategy. In order to simulate realistic irradiance data, the solar data from 06:40 AM to 11:30 AM of July 25th, 2008 in Golden, CO, USA were used based on the data provided by the Solar Radiation Research Laboratory (SRRL) Atmospheric Optical Calibration System (AOCS) of the National Renewable Energy Laboratory [50]. In this case, only PV cluster 1 was connected to the system by closing SW 1, while SW 2 and SW 3 were opened. As it was assumed that the system was connected to a fixed load in this case, the battery current also follows the variation trend similar to the irradiance data. The positive battery current in Fig. 10 denotes that the battery is charged by PV modules. In order to observe the difference in system performance caused by the proposed power management approach, the HPS system was simulated with and without the proposed power management approach. In particular, the main difference to be observed is in the battery current value and the battery temperature. The system performance of the proposed power management approach is shown in Fig. 10(a). Initially, the PV sources operate in the MPP mode so that the system load can be operated and the battery can be charged. Once the battery current value exceeds the pre-set threshold value, $I_{BS}$ = 5 A, the PV sources transit to PR mode according to the proposed power management approach. In the PR mode, only a portion of the available maximum solar power is used as shown in the power plot and the power difference plot of Fig. 10(a). For instance, the apparent discrepancy between the maximum solar power value and the power command value from 9:00 to 11:00 in Fig. 10(a) implies that the PV module output power is regulated to follow a drooped power command instead of the maximum solar power. In Fig. 10, the power difference is defined as the difference between the available maximum solar power (i.e., Eq. (3)) and the actual power command calculated by the power command law (i.e., Eq. (7)). The operation of PR mode can also be implied from the non-zero power difference between the maximum solar power and the actual power command. Accordingly, the battery current does not exceed the battery current threshold value ($I_{BF}$ = 10 A) throughout the overall simulation period. The same system without the proposed power management approach was also simulated with identical irradiance variation data as shown in Fig. 10(b). In this case, the PV modules were controlled to operate always in the MPP mode, while the load was also fixed. As shown in Fig. 10(b), the power command tracks the maximum power value and the power difference between the available power and the power command is zero throughout the simulation. While the battery current does not exceed the value $I_{BF}$ = 10 A in Fig. 10(a), the battery current of Fig. 10(b) increases up to 15 A. As the battery current level depends on the difference between the PV generated power and the load power, the battery current shows a larger increase in Fig. 10(b) as the entire maximum solar power is supplied to the system. Although identical irradiance variation data were used for both simulation cases (i.e., Fig. 10(a) and (b)), the proposed power management approach operated in a manner such that only a portion of the maximum available solar power is transferred to the HPS as shown in Fig. 10(a).

The effect of such high battery current can also be observed from the difference in the battery temperature between Fig. 10 (a) and (b). In the simulation, it was assumed that the battery shell temperature is identical to the ambient temperature (25 °C). To simulate the battery temperature, the battery thermal model of Eq. (10) was considered using the coefficient values of [39] (i.e., $C_b$ = 264.7 and $k$ = 1.286). From Fig. 10, the battery temperature of Fig. 10(b) shows a larger rise compared with the results of Fig. 10(a). The battery temperatures at the end of the simulation in Fig. 10(a) and (b) are approximately 26 °C and 30 °C, respectively. As the same battery was used in both simulation cases, such difference can be explained by the higher battery current value in Fig. 10(b). As introduced in the previous section, the battery performance and safety is strongly affected by the battery temperature. The importance and technical value of the current limiting capability, which is performed by the proposed power management approach without a separate centralized controller in this study, can be highlighted from the observation that the battery temperature rise is limited as in Fig. 10(a). Since battery operation at high temperatures could be prevented by the proposed power management approach, it is possible to prevent performance (e.g., life cycle and capacity) degradation of batteries. Preventing degradation of the battery, which is a critical component to satisfactory operation of HPSs, would contribute to improving reliability as the hardware components of an HPS can have a longer life-cycle compared with an HPS that has a battery with degraded performance. In addition, proper management of the battery would ensure that the HPS could operate in satisfactory and safe manner throughout the operation period. As mentioned in Section 3.2, temperature management is a task that is commonly required for batteries [13,40]. The results of Fig. 10 show that both charge rate limitation and temperature management are performed by adopting the proposed power management approach.

Fig. 11(a) shows the performance of the proposed HPS with different load conditions. As in the previous case, only PV cluster 1 was connected to the system. Until $t$ = 2 min, the battery is being charged with the 3 A charge current. As the battery current is smaller than the threshold value, $I_{BS}$ = 5 A, the PV source operates in the MPP mode, while the power difference between the power generated by the PV source and the power consumed by the load is used for charging the battery. Once the load power decreases at $t$ = 2 min, the battery charging current shows an increase to 7 A. In order to limit the battery charge rate (i.e., battery current), the power output of the PV source decreased according to the adopted power management approach. As shown in the decrease of the PV output power, the PV source operates in the PR mode from $t$ = 2 min to $t$ = 7 min. Although the PV source does not operate in the MPP mode, the PV module can supply sufficient power for load operation and battery charging. Because of the decreased power command value, charging of the energy storage can still be continued at a safe charge rate that prevents the battery current from exceeding the value $I_{BF}$ = 10 A. As soon as the load increases at $t$ = 7 min, the battery discharges the stored energy in order to prevent interruption in load operation. The negative battery current in Fig. 11(a) indicates that the battery is being discharged. Although

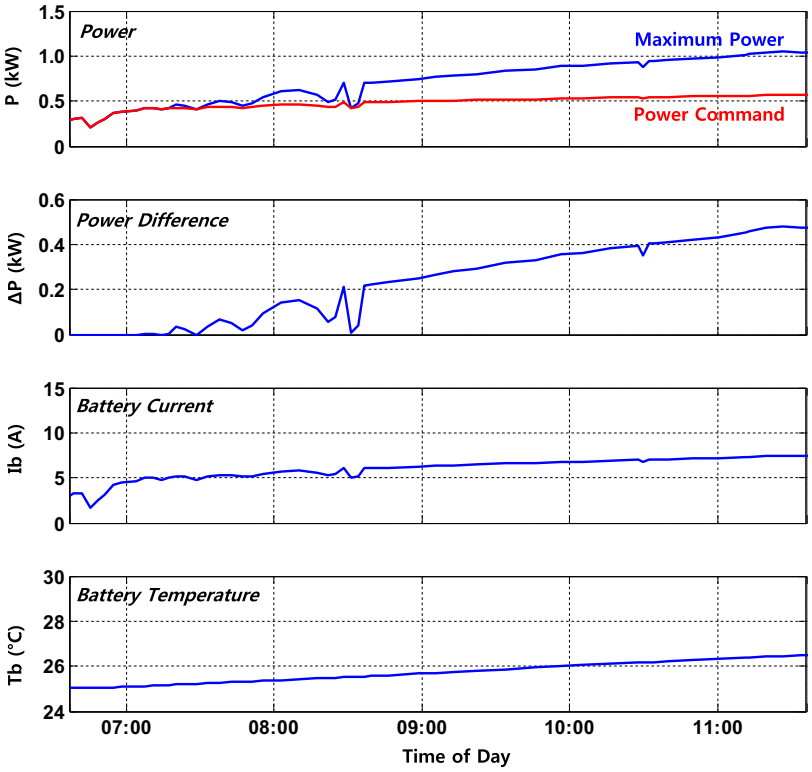


(a) With the proposed power management approach

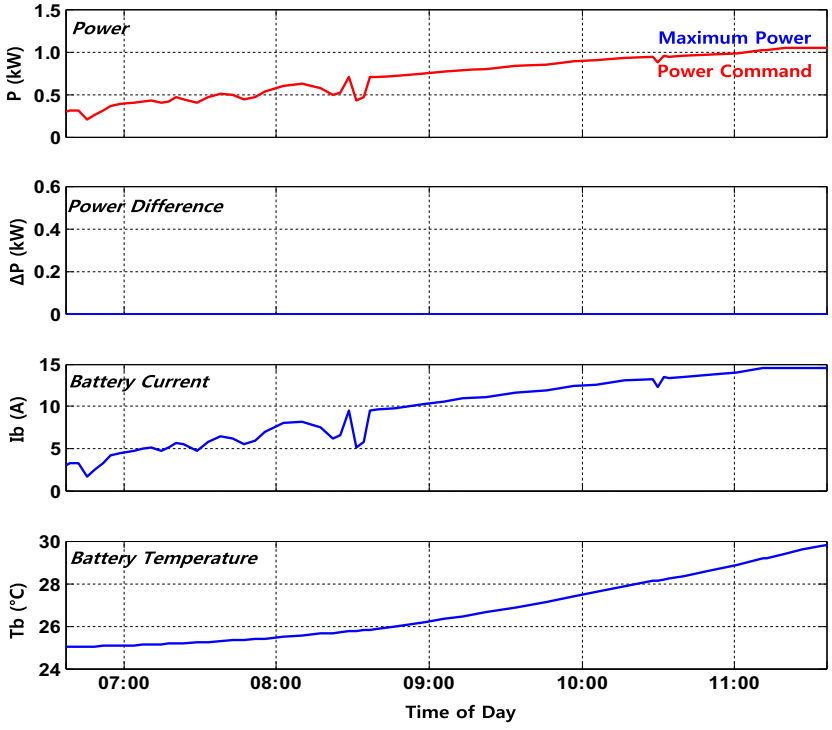


(b) Without the proposed power management approach

**Fig. 10.** Simulation results with different power management approaches.

the PV sources operate in the MPP mode after $t = 7$ min, the load power demand exceeds the PV generated power and the stored energy of the battery should be discharged to the load.

Fig. 11(b) shows the waveforms of the power system after changing the number of PV sources that are connected to the simulated HPS. Initially, only PV cluster 1 is connected to the system

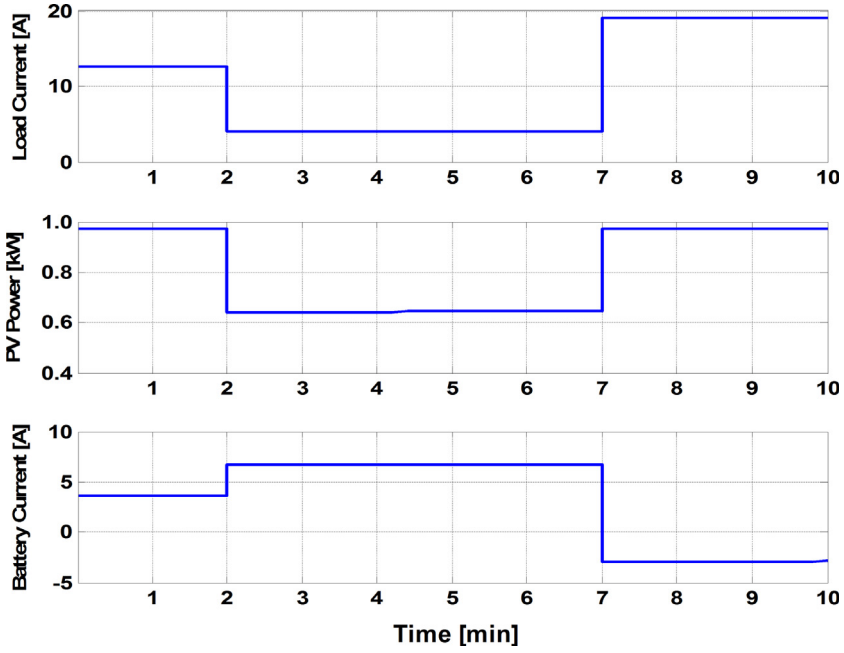


(a) Single PV cluster connected

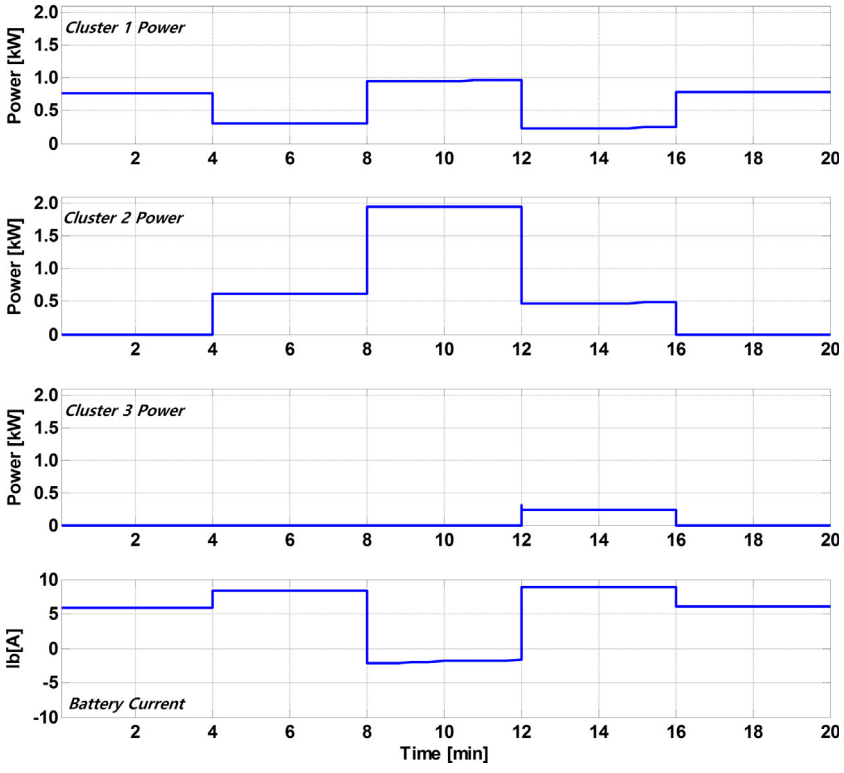


(b) Connection/Disconnection of other PV clusters

**Fig. 11.** Simulation results with the HPS shown in Fig. 9.

by closing SW 1 and leaving the other two switches (i.e., SW 2 and SW 3) open. During this period, the PV modules of PV cluster 1 operate in the PR mode. Once an additional PV source (i.e., PV cluster 2), which has a twice larger power rating than PV cluster 1, is connected by closing SW 2 at $t = 4$ min, it can be seen that the two PV sources both supply power to the battery and load. It is worth noting that the PV clusters supply power to the HPS according to their power ratings. Because of the proposed power management approach, PV cluster 2 supplies twice more power than PV cluster 1. Although the battery charging current increases after connecting an additional power source, the battery current does not exceed the pre-set maximum battery value, $I_{BF} = 10$ A. At $t = 8$ min, the HPS experiences an increase of the load power. Although the PV modules operate at the MPP mode to harvest

the maximum amount of available solar power, the battery experiences a discharge to supply the deficient power to the loads. At $t = 12$ min, the load power decreases and SW3 is also closed so that all three PV clusters are connected. It can be seen that the battery current value is still below the pre-defined threshold value, $I_{BF} = 10$ A, and all three PV clusters supply sufficient power for both load operation and battery charging. Similar to the previous periods (i.e., from $t = 4$ min to $t = 12$ min), the three sources supply the power according to the ratio of power ratings. That is, the output of PV clusters 1 and 3 is identical to each other whereas the output of PV cluster 2 doubles that of the other two PV clusters. In order to verify that the proposed control approach is not affected by the removal of power sources, PV clusters 2 and 3 are disconnected from the main bus as shown in the output power waveforms after $t = 16$ min. As soon as PV clusters 2 and 3 are disconnected, the output of the remaining source (i.e., PV cluster 1) increases so that the load still operates and the battery charging continues. Such a simulation result shows that the change in the number of power sources does not affect the power system performance even without a separate supervisory controller. The waveforms from $t = 4$ min to $t = 16$ min in Fig. 11(b) demonstrate that the power system architecture with the control approach of this study enables scalable operation of PV-battery HPSs by showing that the variation in the size of the PV sources does not affect the system performance (i.e., proportional power sharing between different PV sources and preventing occurrence of an excessively large battery current).

## 6. Conclusion

This paper introduced the design and control of a PV-battery hybrid power system (HPS). In order to effectively address the intermittent characteristics of PV sources and uncertainty in load profiles, this paper adopted a power architecture that connects the battery directly to the main system bus of the HPS. A decentralized power management approach was proposed to enable reliable and scalable operation. The PV sources operate as a current source, while the PV sources are commanded to supply either the maximum available power or a drooped power command determined by the battery current. The proposed control approach controls both the power flow and the battery current without requiring explicit feedback of the load power information. A quantitative reliability analysis that uses hardware failure rate data was performed to demonstrate advantages of adopting a passively connected energy storage configuration from a reliability perspective. The analysis result showed that the considered configuration prevents the HPS from being affected by failures of the power electronics interface for energy storage connection. The performance of the system was verified by simulating the HPS using actual solar irradiance profiles and a thermal model of the battery. The verification results showed that the proposed HPS can be effectively managed to accommodate power mismatches and system expansion needs in a decentralized manner. Furthermore, the proposed power management approach contributes to improving reliability by preventing the battery from experiencing excessive charge rates and thermal stress.

This paper contributes to the field of HPS design and control by introducing an approach that enables higher level of reliability and scalability. The results of the quantitative reliability analysis show the possibility to operate an HPS with higher hardware reliability level. As the HPS can be controlled without extensive communication between units of the HPS, a more reliable system operation is possible compared with centralized system control approaches. Because of the decentralized approach, the proposed HPS can also be easily scaled to allow further connections of sources, while preserving both the load sharing performance and battery charge current limit. Hence, the proposed design and power management approach enables reliable and scalable operation of PV-battery HPSs. Based on the promising results of this research, future work could be performed on developing detailed control approaches for an HPS that is connected to power grids and exploring the effect of different energy storage technologies to the HPS performance.

## Acknowledgement

This research was supported by Basic Science Research Program through the National Research Foundation of Korea (NRF) funded by the Ministry of Science, ICT and Future Planning (NRF-2014R1A1A1036384).

## References

[1] Kaabeche A, Ibtiouen R. Techno-economic optimization of hybrid photovoltaic/wind/diesel battery generation in a stand-alone power system. Sol Energy 2014;103:171–82.
[2] Bianchi M, Branchini L, Ferrari C, Melino F. Optimal sizing of grid-independent hybrid photovoltaic–battery power systems for household sector. Appl Energy 2014;136(31):805–16.
[3] Wu Z, Tazvinga H, Xia X. Demand side management of photovoltaic-battery hybrid system. Appl Energy 2015;148(15):294–304.
[4] Qi Z, Lin E. Integrated power control for small wind power system. J Power Sources 2012;217:322–8.
[5] Ma T, Yang H, Lu L. A feasibility study of a stand-alone hybrid solar–wind–battery system for a remote island. Appl Energy 2014;121:149–58.
[6] Sun H, Luo X, Wang J. Feasibility study of a hybrid wind turbine system – integration with compressed air energy storage. Appl Energy 2015;137:617–28.
[7] Bernard J, Hofer M, Hannesen U, Toth A, Tsukada A, Buchi F, et al. Fuel cell/battery passive hybrid power source for electric powertrains. J Power Sources 2011;196:5867–72.
[8] Ettihir K, Boulon L, Agbossou K. Optimization-based energy management strategy for a fuel cell/battery hybrid power system. Appl Energy 2016;163:142–53.
[9] Fadel A, Zhou B. An experimental and analytical comparison study of power management methodologies of fuel-cell battery hybrid vehicles. J Power Sources 2011;196:3271–9.
[10] Thounthong P, Rael S, Davat B. Control algorithm of fuel cell and batteries for distributed generation system. IEEE Trans Energy Convers 2008;23(1):148–55.
[11] Song Z, Hofmann H, Li J, Hou J, Han X, Ouyang M. Energy management strategies comparison for electric vehicles with hybrid energy storage system. Appl Energy 2014;134:321–31.
[12] Castaings A, Lhomme W, Trigui R, Bouscayrol A. Comparison of energy management strategies of a battery/supercapacitors system for electric vehicle under real-time constraints. Appl Energy 2016;163:190–200.
[13] IEEE guide for optimizing the performance and life of lead-acid batteries in remote hybrid power systems. IEEE Std. 1561–2007.
[14] Valenciaga F, Puleston P. Supervisor control for a stand-alone hybrid generation system using wind and photovoltaic energy. IEEE Trans Energy Convers 2005;20(2):398–405.
[15] Wang G, Chobotaru M, Agelidis VG. Power smoothing of large solar PV plant using hybrid energy storage. IEEE Trans Sustainable Energy 2014;5(3):834–42.
[16] Syed IM, Raahemifar K. Predictive energy management and control system for PV system connected to power electric grid with periodic load shedding. Sol Energy 2016;136:276–87.
[17] Tazvinga H, Zhu B, Xia X. Energy dispatch strategy for a photovoltaic-wind-diesel-battery hybrid power system. Sol Energy 2014;108:412–20.
[18] Sergi F, Andaloro L, Napoli G, Randazzo N, Antonucci V. Development and realization of a hydrogen range extender hybrid city bus. J Power Sources 2014;250:286–95.
[19] Simmons K, Guezennec Y, Onori S. Modeling and energy management control design for a fuel cell hybrid passenger bus. J Power Sources 2014;246:736–46.
[20] Verstraete D, Lehmkuehler K, Gong A, Harvey J, Brian G, Palmer J. Characterization of a hybrid, fuel-cell-based propulsion system for small unmanned aircraft. J Power Sources 2014;250:204–11.
[21] Lee B, Kwon S, Park P, Kim K. Active power management system for an unmanned aerial vehicle powered by solar cells, a fuel cell, and batteries. IEEE Trans Aerospace Electron Syst 2014;50(4):3167–76.
[22] de la Parra I, Marcos J, Garcia M, Marroyo L. Control strategies to use the minimum energy storage requirement for PV power ramp-rate control. Sol Energy 2015;111:332–43.
[23] Ma T, Yang H, Lu L. Development of hybrid battery-supercapacitor energy storage for remote area renewable energy systems. Appl Energy 2015;153:56–62.
[24] Zhao C, Yin H, Ma C. Quantitative efficiency and temperature analysis of battery-ultracapacitor hybrid energy storage systems. IEEE Trans Sustainable Energy 2016;7(4):1791–802.

[25] Kishizawa A, Kallo J, Garrot O, Weiss-Ungethum J. Fuel cell and Li-ion battery direct hybridization system for aircraft applications. J Power Sources 2013;222:293–300.
[26] Vandoorn T, Meersman B, Kooning J, Vandevelde L. Analogy between conventional grid control and islanded microgrid control based on a global dc-link voltage droop. IEEE Trans Power Delivery 2012;27(3):1405–14.
[27] Villalva M, Gazoli J, Filho E. Comprehensive approach to modeling and simulation of photovoltaic arrays. IEEE Trans Power Electron 2009;24 (5):198–208.
[28] Coelho R, Concer F, Martins D. A MPPT approach based on temperature measurements applied in PV systems. In: 9th IEEE/IAS international conference on industry applications; 2010. p. 1–6.
[29] Sera D, Teodorescu R, Rodriguez P. PV panel model based on datasheet values. IEEE Int Symp Ind Electron 2007:2392–6.
[30] Silva EA, Bradaschia F, Cavalcanti MC, Jascimentro Jr AG. Parameter estimation method to improve the accuracy of photovoltaic electrical model. IEEE J Photovoltaics 2016;6(1):278–85.
[31] Dragicevic T, Vasquez J, Guerrero J, Skrlec D. Advanced LVDC electrical power architectures and microgrids. IEEE Electrification Mag 2014;2(1):54–65.
[32] Kasper M, Burkart RM, Deboy G, Kolar JW. ZVS of power MOSFETs revisited. IEEE Trans Power Electron 2016;31(12):8063–7.
[33] Rabkowski J, Peftitsis D, Nee H-P. Silicon carbide power transistors: a new era in power electronics is initiated. IEEE Ind Electron Mag 2012;6(2):17–26.
[34] Ahadi A, Ghadimi N, Mirabbasi D. Reliability assessment for components of large scale photovoltaic systems. J Power Sources 2014;264:211–9.
[35] Rausand M, Holyland A. System reliability theory: models, statistical methods, and applications. 2nd ed. Wiley-Interscience; 2004.
[36] Guerrero J, Vasquez J, Matas J, Vicuna L, Castilla M. Hierarchical control of droop-controlled AC and DC microgrids-a general approach toward standardization. IEEE Trans Ind Electron 2011;58(1):158–72.
[37] Tonkoski R, Lopes L, El-Fouly T. Coordinated active power curtailment of grid connected PV inverters for overvoltage prevention. IEEE Trans Sustainable Energy 2011;2(2):139–47.
[38] Battery charging. Texas instruments technical document (SNVA557); 2011.
[39] Zhang C, Li K, Deng F. Real-time estimation of battery internal temperature based on a simplified thermoelectric model. J Power Sources 2016;302:146–54.
[40] Linden D, Reddy TB. Handbook of batteires. 3rd ed. McGraw-Hill; 2002.
[41] Cao J, Emadi A. Batteries need electronics. IEEE Ind Electron Mag 2011:27–35.
[42] Gagne A, Turcotte D, Goswamy N, Poissant Y. High resolution characterization of solar variability for two sites in Eastern Canada. Sol Energy 2016;137:46–54.
[43] Belhachat F, Larbes C. Modeling, analysis and comparison of solar photovoltaic array configurations under partial shading conditions. Sol Energy 2015;120:399–418.
[44] Sun J. Impedance-based stability criterion for grid-connected inverters. IEEE Trans Power Electron 2011;26(11):3075–8.
[45] Wen S, Lan H, Hong Y-Y, Yu DC, Zhang L, Cheng P. Allocation of ESS by interval optimization method considering impact of ship swinging on hybrid PV/diesel ship power system. Appl Energy 2016;175:158–67.
[46] Xiong X, Tse CK, Ruan X. Bifurcation analysis of standalone photovoltaic-battery hybrid power system. IEEE Trans Circuits Syst-I: Regular Papers 2013;60(5):1354–65.
[47] Zhang X, Ruan X, Tse CK. Impedance-based local stability criterion for DC distribution power systems. IEEE Trans Circuits Systems-I: Regular Papers 2015;62(3):916–25.
[48] Kwasinski A, Onwuchekwa CN. Dynamic behavior and stabilization of DC microgrids with instantaneous constant-power loads. IEEE Trans Power Electron 2011;26(3):822–34.
[49] KYOCERA corporation. KC 200GT specification sheet. Available from: http://www.kyocerasola.com/assets/001/5195.pdf. [accessed 01.03.16].
[50] Solar data sets from the SRRL AOCS (solar radiation research laboratory atmospheric optical calibration system) at the national renewable energy laboratory (NREL). Available from http://www.nrel.gov/midc/srrl_aocs/. [accessed 03.29.16].